Manufacturing Rev. **11**, 18 (2024)
https://doi.org/10.1051/mfreview/2024017

Manufacturing Review
Available online at:
https://mfr.edp-open.org

RESEARCH ARTICLE OPEN ACCESS

Synthesis nano core-shell material Fe_3O_4@SiO_2 for magnetorheological finishing with Halbach array and regenerative abrasive system

Nguyen Ngoc Quan, Nguyen Minh Quang, Le Thi Phuong Thanh, Nguyen Tien Tung, Tran Ngoc Tan, and Nguyen Duy Trinh*

Hanoi University of Industry, Tu Liem District, Ha Noi, Vietnam

Received: 28 February 2024 / Accepted: 8 July 2024

Abstract. Fe_3O_4@SiO_2 nanomaterials hold significant promise for diverse applications across various fields. This study aims to elucidate the feasibility and effectiveness of Fe_3O_4@SiO_2 in surface finishing processes. Utilizing the co-precipitation method, SiO_2 shells were successfully coated onto Fe_3O_4 nanoparticles. The abrasive properties of Fe_3O_4@SiO_2 were analyzed for their efficiency in surface finishing. Leveraging the magnetic field generated by a Halbach array, combined with an abrasive particle replacement system, we propose a robust and highly effective polishing process using Fe_3O_4@SiO_2 abrasives. This study details the formation of a magnetorheological fluid (MRF) polishing tool incorporating Fe_3O_4@SiO_2 abrasive particles. Practical experiments were conducted on Sapphire workpieces to validate the proposed polishing process. The experimental setup was designed to assess the surface finishing capabilities and material removal behaviour. Results demonstrated that the Sapphire surface achieved nanometer-scale smoothness with a roughness average (Ra) of 1.145 nm, free of surface damage, after just 100 min of processing. The underlying mechanisms of material removal were also investigated and discussed. The findings suggest that MRF polishing using Fe_3O_4@SiO_2 abrasive particles is a promising and efficient method for surface finishing across various materials.

Keywords: Nanomaterials / Fe_3O_4@SiO_2 / magnetorheological fluid polishing / Halbach array / sapphire material / abrasive replacement system / finite element analysis

1 Introduction

With advancements in science and technology, the significance of surface quality in machined components has become increasingly paramount across various fields. The interaction of a component with its surrounding environment and its overall functional performance is predominantly influenced by surface properties [1,2]. This directly influences the material's interaction with the environment, as well as its durability and mechanical properties. Enhancing surface quality yields multiple benefits, including reduced friction, increased longevity, improved cleanability, and notably, enhanced functional performance of the product [3,4]. In the context of increasing demands for higher quality and efficiency in machinery, equipment, and products, the need for achieving nanometer-level surface finishes post-machining has become exceedingly urgent. Recently, various polishing technologies such as mechanical-chemical polishing, electrochemical polishing, laser polishing, and magnetorheological polishing have been developed and implemented [5–7]. Among these, magnetorheological fluid (MRF) polishing stands out as one of the most effective methods for achieving superior surface quality. This process utilizes the interaction between a magnetic field and a magnetic material to propel abrasive particles against the machined surface, effectively removing residual material [8,9]. The efficacy of the MRF process is predicated on the magnetorheological effect of the MR polishing solution when exposed to a magnetic field [10]. MRF fluids typically consist of carbonyl iron particles (CIPs), non-magnetic abrasives, deionized water, or other fluids. During the process under the influence of a magnetic field, the CIPs will form clusters along the magnetic field lines and pull non-magnetic abrasive particles onto the workpiece surface [11,12]. This characteristic enables the MRF polishing method to meet diverse requirements by precisely removing a determined amount of residual material without causing any surface damage [13].

In recent years, Halbach arrays have drawn significant attention from researchers in physics and mathematics due

* e-mail: duytrinh99@gmail.com

to their remarkable capability to enhance magnetic field distribution within electromagnetic systems [14]. Comprising alternating primary and transition permanent magnets, Halbach arrays can adopt linear or circular configurations [15]. A defining characteristic of Halbach arrays lies in their unique ability to generate a robust, concentrated magnetic field on one side (referred to as the active side), while simultaneously reducing it on the opposite side (known as the quiet side) [16]. This attribute substantially strengthens the operational effectiveness of systems wherein they are deployed. In the context of magnetic polishing processes, the Halbach array assumes a pivotal role by optimizing magnetic force within the polishing area [17,18]. This optimization is particularly crucial as it enables precise control over magnetic field forces, facilitating the attainment of superior surface finishes [19]. By bolstering magnetic force within the active zone, the Halbach array significantly enhances polishing performance, thereby reducing the time and resources expended to achieve desired outcomes [18,20]. Consequently, this augmentation can yield increased operational efficiency and reduced overhead costs in industrial settings [21]. Furthermore, the Halbach array contributes to the refinement of the polishing process by mitigating magnetic field disturbances on the quiet side [22]. This mitigation is instrumental in enhancing the process's precision and reliability, especially in applications necessitating meticulous accuracy, such as the MRF polishing of optical and electronic components [23]. The Halbach array plays a crucial role in enhancing the efficiency and precision of magnetic polishing processes [24]. Its capability to produce a strong, focused magnetic field on the active side, while simultaneously minimizing magnetic field intensity on the quiet side, not only improves polishing efficiency but also opens up numerous potential applications across various high-tech domains [25].

In MRF polishing processes, non-magnetic abrasives are frequently incorporated into the MR fluid to address the inherently low material removal rate (MRR). These abrasive particles can enhance the mechanical grinding effect due to their high hardness or decrease the hardness of the material surface via chemical reactions during polishing. Incorporating silica abrasives into the MR fluid containing carbonyl iron (CI) powder not only improves surface quality but also enhances the MRR of the polished material surface in MRP [26]. However, non-magnetic abrasive particles tend to agglomerate or be lost in the polishing area, resulting in an uneven surface distribution of the polished material. To address this issue, composite abrasive particles that integrate non-magnetic and magnetic abrasives have been developed. Pan et al. [27] developed SiO_2/CI composite abrasives for the MRP process of sapphire wafers, with experimental results indicating that these composite abrasives significantly enhance surface quality and finishing efficiency for sapphire materials. Zhai et al. [28] developed Fe_3O_4/SiO_2 composite abrasives for the MRF polishing process, where core-shell abrasives demonstrated superior polishing performance compared to pure Fe_3O_4 particles and Fe_3O_4-SiO_2 mixed abrasives. They also established mathematical models for normal force, shear force, and MRR in the polishing process.

Pressure and shear stress are both critical factors in the material removal process during MRF. Shorey measured forces in MRF and concluded that material removal rate (MRR) is more influenced by drag force than by normal load [29]. Building upon Shorey's findings, Degroote developed a comprehensive model to predict the MRR of optical components, incorporating factors such as the mechanical properties of the glass, drag forces, and the characteristics of the polishing abrasives. In this model, MRR is defined as a function of the drag force [30,31]. Additionally, Miao's research demonstrated a positive correlation between MRR and shear stress [32]. Several studies have emphasized that pressure should not be overlooked in MRR prediction. Kum proposed a semi-empirical model for MRR in magnetic finishing processes, derived from experimental methods, which revealed a strong correlation between MRR and tangential force [30]. Both pressure and shear stress influence MRR, with shear stress being the dominant factor; however, as immersion depth increases, the contribution of pressure to MRR becomes more significant [30].

This study addresses the limitations of traditional MRF processes by exploring the application of Fe_3O_4@-SiO_2 nanomaterials in ultra-precision machining. The authors investigate the potential of these magnetized core-structured nanomaterials as abrasive agents, aiming to enhance the bonding ability within the polishing solution compared to conventional MRF processes. A Halbach magnetic field array is employed to generate a robust magnetic field in the machining area, and an abrasive regeneration system utilizing a conveyor belt is introduced to ensure continuous renewal of abrasive particles on the machined surface. This article first outlines the synthesis process of Fe_3O_4@SiO_2 materials. Subsequently, it presents the development of a polishing model incorporating these abrasives and the regeneration system. Theoretical analysis and finite element methods are used to examine the magnetic field generation through the Halbach array, operating principles, and material removal methods. Practical experiments on sapphire material are conducted to assess the surface finishing capabilities of the Fe_3O_4@SiO_2 abrasives in the MRF process. Additionally, the study provides a detailed analysis of the material removal mechanism by considering the polishing zone and the shear stress within it.

2 Synthesis of Fe_3O_4@SiO_2 material

Raw materials used include Ethanol (C_2H_5OH), Iron(II) chloride tetrahydrate ($FeCl_2{\cdot}4H_2O$), Tetraethyl orthosilicate (TEOS, chemical formula $Si(OC_2H_5)_4$ or $SiC_8H_{20}O_4$), Sodium hydroxide (NaOH), Iron(III) chloride hexahydrate ($FeCl_3.6H_2O$), Ammonia (NH3), distilled water. All chemicals were used directly without further purification during the experimental procedures.

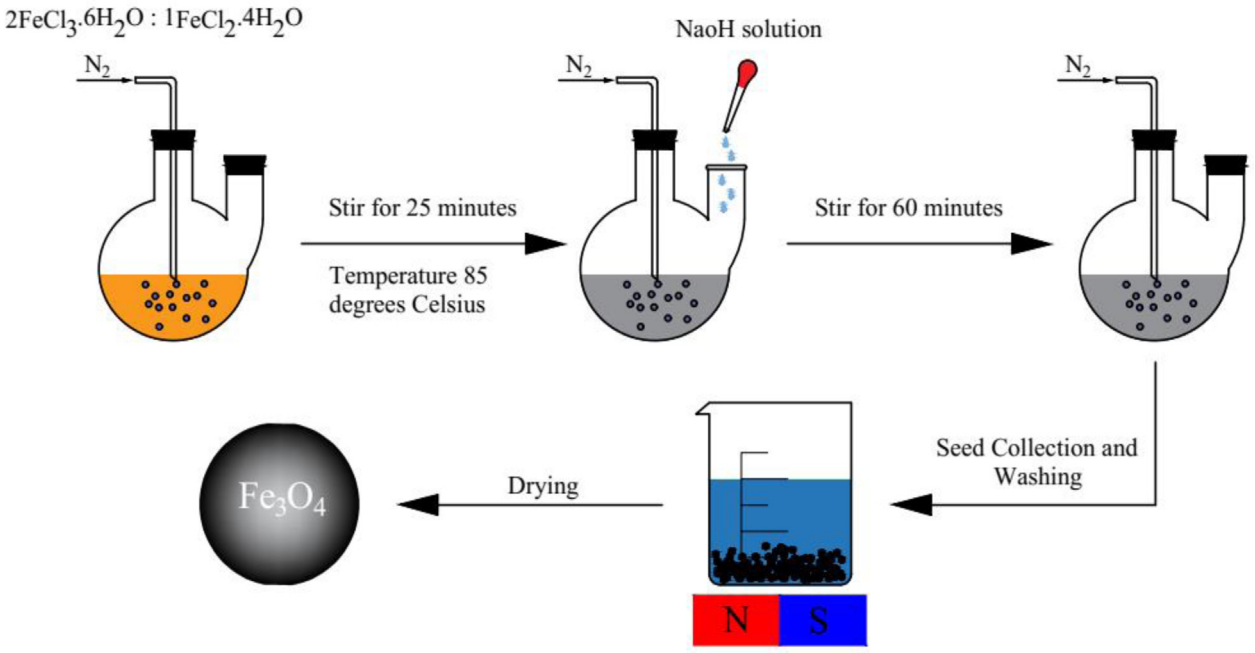

Fig. 1. Synthesis process of Fe_3O_4 nanoparticles.

2.1 Synthesis of Fe_3O_4

The Fe_3O_4 synthesis process includes many steps, Figure 1 shows the synthesis process on Fe_3O_4 nanoparticles. The determination of the contents and ratios of the constituent elements in Fe_3O_4 was achieved through careful stoichiometric calculations based on the molar ratios of the reactants. First, prepare a spherical flask with 50 mL of deionized water, then add a mixture of $FeCl_3{\cdot}6H_2O$ and $FeCl_2{\cdot}4H_2O$ with a molar ratio of 2:1 to it. Stir the mixture for 25 min with the help of a stirrer. While this process is carried out to prevent oxidation, N_2 gas is continuously supplied until particles are formed and the temperature of the solution is reached. Salt also slowly provides a certain temperature. After reaching the temperature of 85 °C, slowly add NaOH solution to the mixture in the molar ratio of $8OH^-$:$2Fe^{2+}$:$1Fe^{3+}$. Finally, wait until the reaction is complete and stir the mixture for 60 min, then perform the process of collecting nanoparticles by placing the cup on a magnet, then washing the mixture with C_2H_5OH and deionized water to Remove salt from nanoparticles, with the impact of a magnet, in this process the nanoparticles are retained. Finally, these particles are dried at a temperature of 70 °C and the result is Fe_3O_4 nanoparticles [33]. The process of creating Fe_3O_4 nanoparticles is expressed through the following two equations:

$$8\text{NaOH}+\text{FeCl}_2 + 2\text{FeCl}_3 \rightarrow \text{Fe}_{(\text{OH2})} + 2\text{Fe(OH)}_3, \quad (1)$$

$$\text{Fe(OH)}_2 + 2\text{Fe(OH)}_3 \rightarrow \text{Fe}_3\text{O}_4 + 4\text{H}_2\text{O}. \quad (2)$$

2.2 Synthesis of core–shell structure Fe_3O_4@SiO_2 material

The process of synthesizing Fe_3O_4@SiO_2 material and determining the ratio of the constituent elements is based on a well-established procedure. The chemical ratios used in the synthesis are crucial for achieving uniform and controlled SiO_2 shell thickness, which is essential for the performance of Fe_3O_4@SiO_2 in MRF applications. Study by Nyiro-Kosa et al. [34] provides a detailed method to control the shell thickness by adjusting the amount of TEOS added to the reaction mixture. The process of creating the core-shell structure Fe_3O_4@SiO_2 material is shown in Figure 2. First, ferromagnetic nanoparticles are mixed with C_2H_5OH, NH_3, H_2O in a ratio of 1:10:30:50 [10]. Then, the mixture was subjected to ultrasonic vibration for 35 min, then TEOS was slowly added into the mixture at a ratio of 1:90 and continued to stir for 480 min. Through the condensation and hydrolysis of TEOS, the SiO_2 layer was created and adhered to the ferromagnetic nanoparticles. Similar to the way iron nanoparticles are collected from SiO_2-coated Fe_3O_4 nanoparticles are collected by placing the cup on a magnet and then washing the mixture with C_2H_5OH and deionized water. Finally, the nanoparticles were dried at a temperature of 65 °C and the result was a

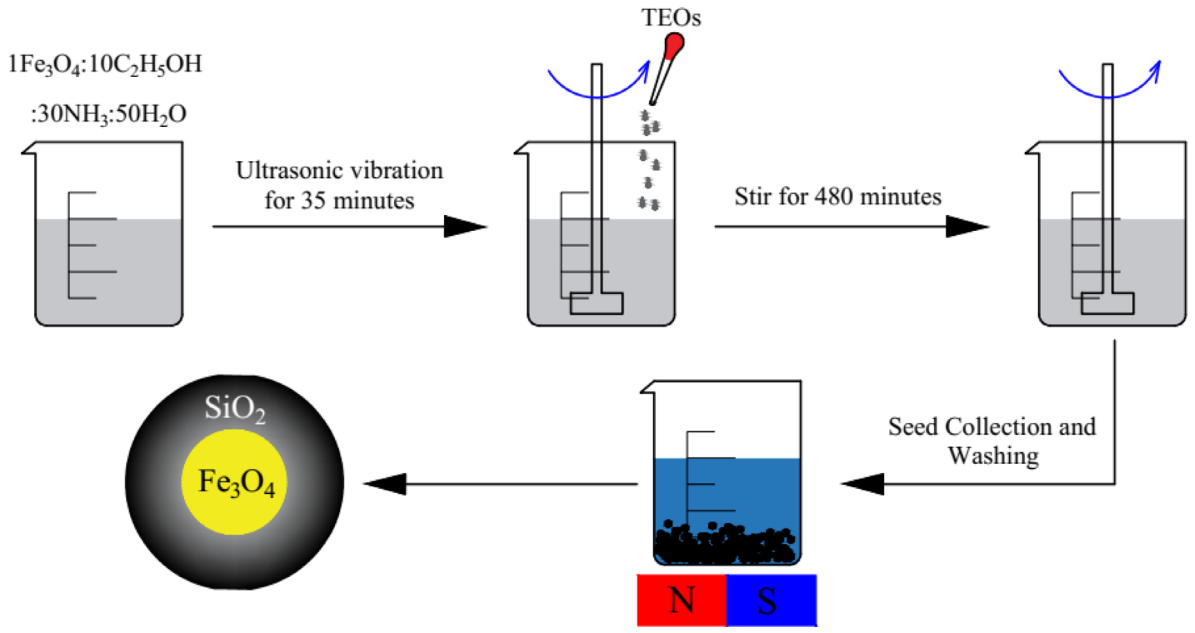

Fig. 2. Synthesis process of Fe_3O_4@SiO_2 nanomaterial with core-shell structure.

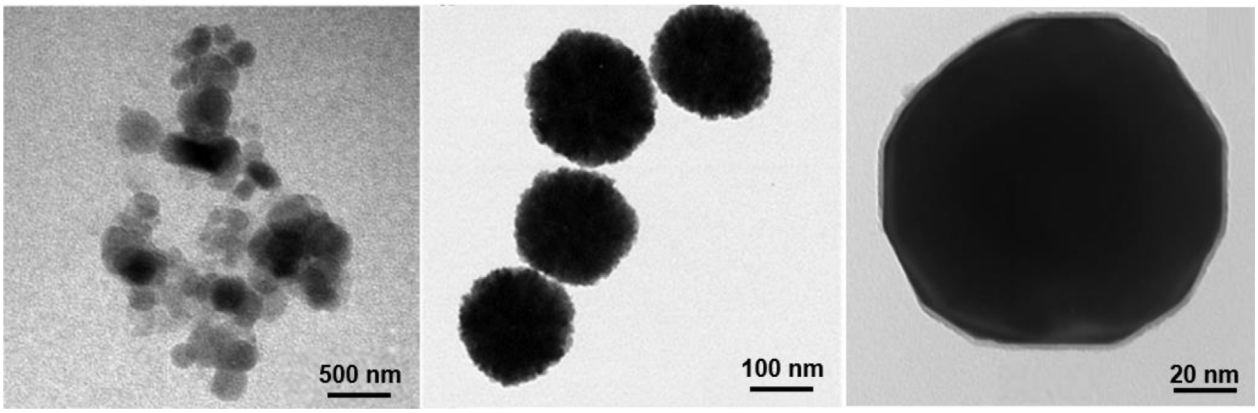

Fig. 3. TEM image of Fe_3O_4@SiO_2 nanoparticles [37].

Fe_3O_4@SiO_2 nanomaterial with a core-shell structure [35,36]. Figure 3 shows the image of Fe_3O_4@SiO_2 particles.

3 Materials and methods

3.1 Equipment diagram and method of removing excess material

Figure 4 illustrates the schematic diagram of the MRF polishing equipment. The setup comprises three main components: the magnetic excitation unit, the abrasive particle replacement system, and the rotary motion generator for the workpiece. The abrasive particle replacement system features a conveyor belt connected to a motor via a belt drive. Additionally, this system incorporates a throttle valve and a peristaltic pump, which facilitate the transfer of the MRF solution from the supply tank and the collection of abrasive particles at the end of the conveyor belt. The magnetic excitation unit consists of a circular Halbach array mounted on a shaft, secured in position by two aluminium rods. For the workpiece motion mechanism, the workpiece is fixed in place using a jig, which is connected to the motor via a belt drive.

Figure 5 shows the principle and method of removing excess material of the MRF process with Fe_3O_4@SiO_2 abrasives. When the MRF process is started, first after receiving a rotation from the motor, the active wheel of the conveyor (wheel number 1) rotates and causes the passive wheel of the conveyor belt (wheel number 2). This number 2 wheel is a circular Halbach array, the Halbach array acts as a way to provide a magnetic field during the machining process. As soon as wheel number 2 is brought close to the machining area, the polishing liquid is brought from the tank to the surface of the conveyor belt through the power pump. This polishing liquid mixture consists of Fe_3O_4@SiO_2 abrasive particles and reducing water mixed together. Immediately under the strong impact of the magnetic field, in the machining area, the Fe_3O_4@SiO_2 abrasive particles are tightly held on the conveyor surface and arranged into particle

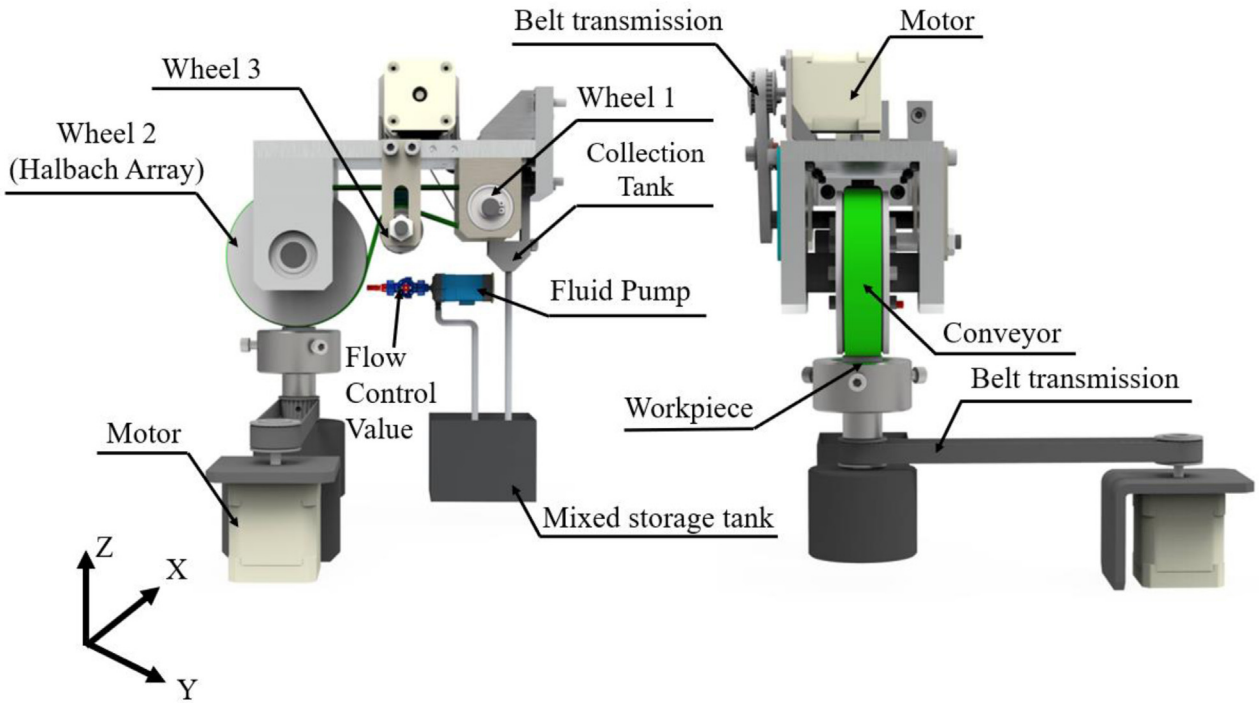

Fig. 4. Diagram of MRF equipment.

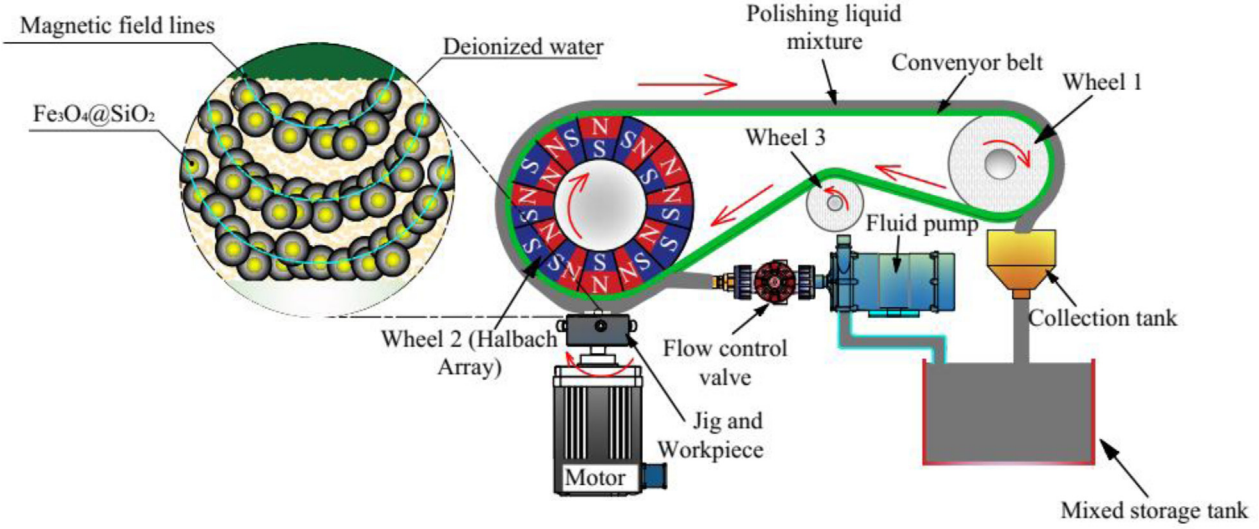

Fig. 5. Processing principles.

clusters along the magnetic field lines. At this time, after the workpiece is provided with rotational motion, through the support of the conveyor belt, $Fe_3O_4@SiO_2$ particle clusters are brought to the surface of the material and perform the task of removing excess material. After performing its task, the MRF polishing solution is taken out of the processing area with the help of a conveyor belt and collected into the storage tank. This process is performed in repeated cycles until the material surface reaches the required quality.

In Figure 5, a cross-sectional view of the polishing wheel equipped with a circular Halbach array is presented. The circular Halbach array is crafted from Nd-Fe-B and boasts an outer diameter of 100 mm, a magnet length of 20 mm. The North and South poles of the magnetic ring are represented by different colors as depicted in Figure 5. Magnets within the Halbach array play a crucial role with positioned circularly and in proximity to the outer edge of the plastic disk. Specifically, the circular Halbach array generates a magnetic field characterized by substantial impact force and a focused direction of impact towards the exterior of the conveyor belt.

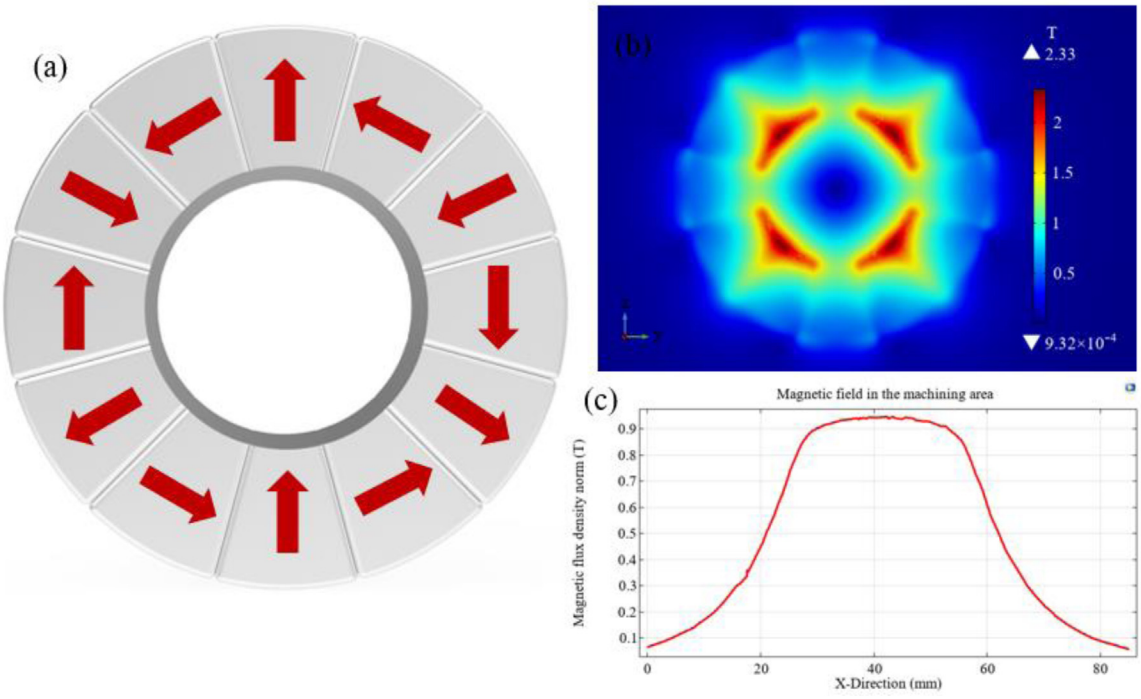

Fig. 6. Details of the Halbach array used.

The green lines in Figure 5 represent the magnetic induction lines, delineating the trajectories along which magnetic particles are attracted and mobilized. Within the machining zone, particles are subjected to forces F_X and F_Y, which are oriented along the magnetic force lines in the x and y directions. These forces constitute the components of the magnetic force exerted on the magnetic particles located on the conveyor belt. The expression for these forces is articulated by the following equation [37]:

$$F_X = \chi \times V \times \mu_0 \left[\frac{H\partial H}{\partial x}\right], \tag{3}$$

$$F_Y = \chi \times V \times \mu_0 \left[\frac{H\partial H}{\partial y}\right], \tag{4}$$

in this context, V represents the volume of the magnetic particle, χ denotes the magnetic susceptibility of the magnetic particle, H and μ_0 magnetic field density and vacuum magnetic permeability. The gradient in the x,y direction is determined by $\frac{\partial H}{\partial x}$, $\frac{\partial H}{\partial y}$. Figure 5 depicts the magnetic force acting on magnetic particles with the formula as described below:

$$F = F_X \times \sin(\gamma_i) + F_Y \times \cos(\gamma_i), \tag{5}$$

in this equation, γ_i tilt angle of the magnetic induction line. The magnetic force is determined by F_M with mathematically expressed as follows:

$$F_M = \frac{3}{2}\mu_0 \times (\pi R^2) \times \left(\frac{X_R^2 H^2}{(3 + X_R)^2}\right), \tag{6}$$

where R represents the radius of the magnetic particle, X_R is the specific susceptibility of the magnetic particle, and m_0 is the magnetic permeability of the vacuum. Through the interaction between magnetic particles and the magnetic field force, the MRF slurry adheres tightly to the belt and moves in alignment with the belt's direction, effectively serving as machining tools to complete the process, as depicted in Figure 5.

3.2 Method of creating a magnetic field

In the pursuit of enhancing the magnetic field strength for optimal efficiency in the MRF process, a magnetic pole arrangement technique known as the Halbach array has been employed. Figure 5 illustrates the characteristics of the Halbach array technique utilized in this study. The selection of the Halbach array stems from its unique structural design, which mitigates energy loss attributed to undesirable magnetic effects while maximizing the utilization of magnets to achieve a stronger magnetic field [38,39]. For this MRF method, the applied Halbach array is made up of different magnets into a ring-shaped

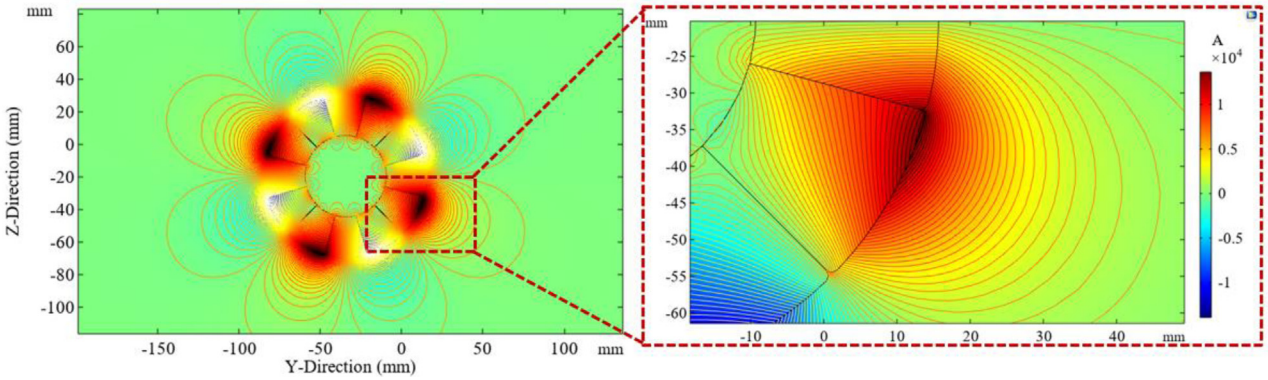

Fig. 7. Distribution of magnetic field.

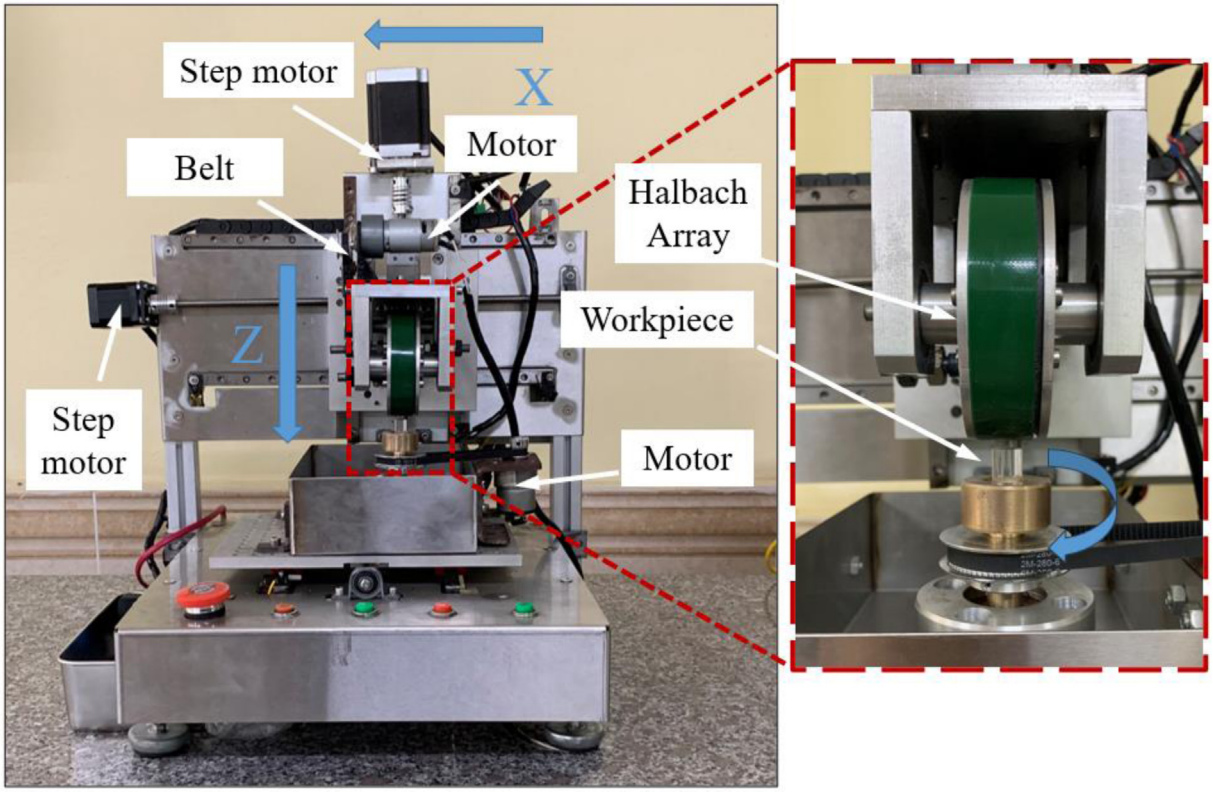

Fig. 8. Experimental equipment.

structure with an outer diameter of 80 mm, a hole diameter of 40 mm and a thickness of 20 mm. The findings are presented in Figure 6a, illustrating the obtained results. Furthermore, Figure 6b provides insight into the magnitude of the magnetic wall generated by the Halbach array. Moreover, Figure 6c showcases the magnitude of the magnetic field within the machining area, revealing a gradual increment with a focal point towards the center. Figure 7 elucidates the distribution of the generated magnetic field lines. As mentioned before, during the implementation process, Fe_3O_4@SiO_2 particle clusters will be formed along the magnetic field lines in the machining area. Through the analysis results from Figures 6c and 7, it can be concluded that while the MRF process is being carried out, in the machining area, Fe_3O_4@SiO_2 abrasive particles will be concentrated and form clusters. has a dome shape and this dome has its peak in the middle of the conveyor belt.

4 Experiment and discussion

In this section, practical experiments were conducted using a lens made from Sapphire material, chosen for its exceptional properties. Sapphire possesses high hardness, abrasion resistance, transparency, and biocompatibility, rendering it indispensable in various fields, particularly in

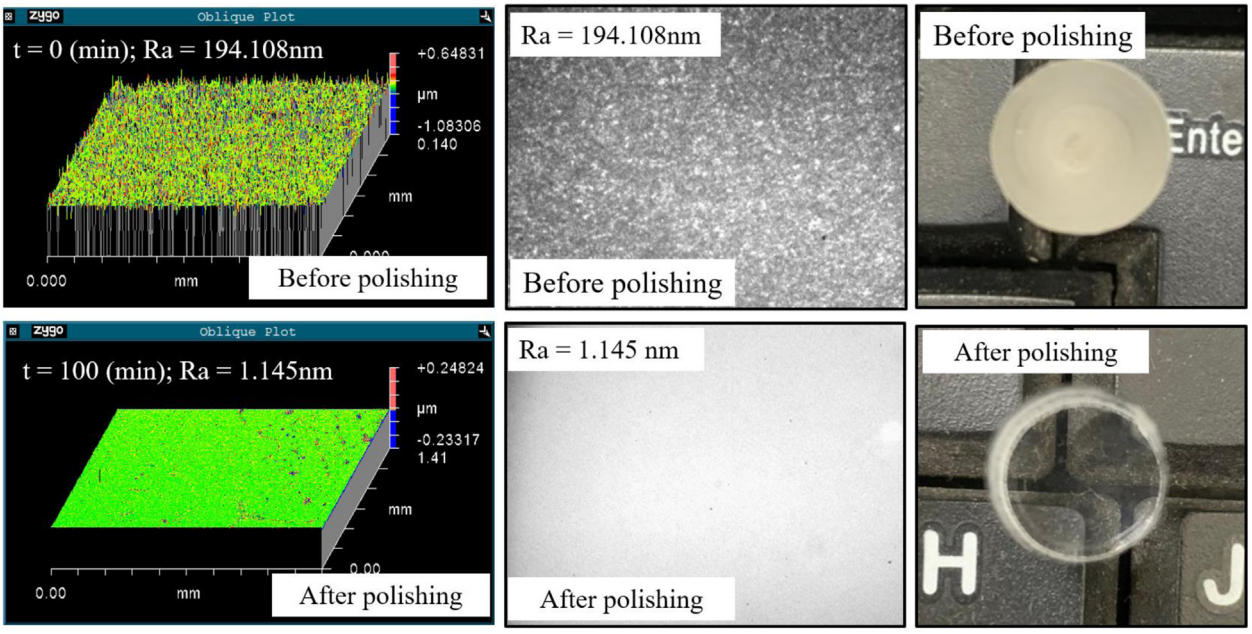

Fig. 9. Effect of Fe_3O_4@SiO_2 in polishing process.

Table 1. Parameters of the experiment.

Parameters	Value	Material	Note
Workpiece		Sapphire	Size: 20 mm × 10 mm
Workpiece velocity	60 rpm		
Linear speed of conveyor belt	150 mm/s		
Working distance	1 mm		
Magnetic field supply method			Halbach array
MRF fluid mixture		Fe_3O_4@SiO_2: 40%;	
Flow rate	15 ml/min	Deionized water: 60%	
Processing time	100 min		

the electronics industry, optics, and numerous other applications. Its versatility renders it a popular choice for applications requiring durability and high quality [40]. The experimental setup employed Sapphire workpieces with a diameter of 20 mm and a thickness of 15 mm. Prior to experimentation, the surface roughness of the material ranged from 150 nm to 250 nm, influenced by preceding processing methods. Subsequent to the polishing process, surface quality was assessed using a Zygo NewView 7100 machine. The actual experimental equipment utilized in accordance with the proposed MRF process diagram is depicted in Figure 8.

4.1 The effectiveness of Fe_3O_4@SiO_2 abrasives in the MRF process

Table 1 shows the specific settings in the experiment to evaluate the effectiveness of Fe_3O_4@SiO_2 abrasive particles. The polishing results with the initial rough workpiece surface and the ultra-smooth surface post-polishing are shown in Figure 9.

The findings from Figure 9 reveal that prior to polishing the Sapphire surface, numerous dense scratches were observed across the entire surface. Particularly evident from the 3D image, the surface exhibited rough, scratch-ridden topography with the surface roughness measured at Ra = 194.108 nm. Following a 100 min polishing process, significant improvements were observed. The surface appeared flatter, brighter, and smoother, with the rough peaks nearly eradicated. The surface roughness was significantly reduced, now measuring Ra = 1.145 nm. This efficiency of the process can be explained by different reasons. Firstly, in the abrasive replacement system, the Fe_3O_4@SiO_2 within the machining area is always renewed throughout the process. Second, applying the Halbach array to polishing helps the whole process always have a stronger magnetic field, increasing the ability to interact with particles in the solution. Third, Fe_3O_4@SiO_2 abrasive particles can be controlled directly by the magnetic field without the need for indirect control through the connection of any other type of particle, eliminating the weakening of the

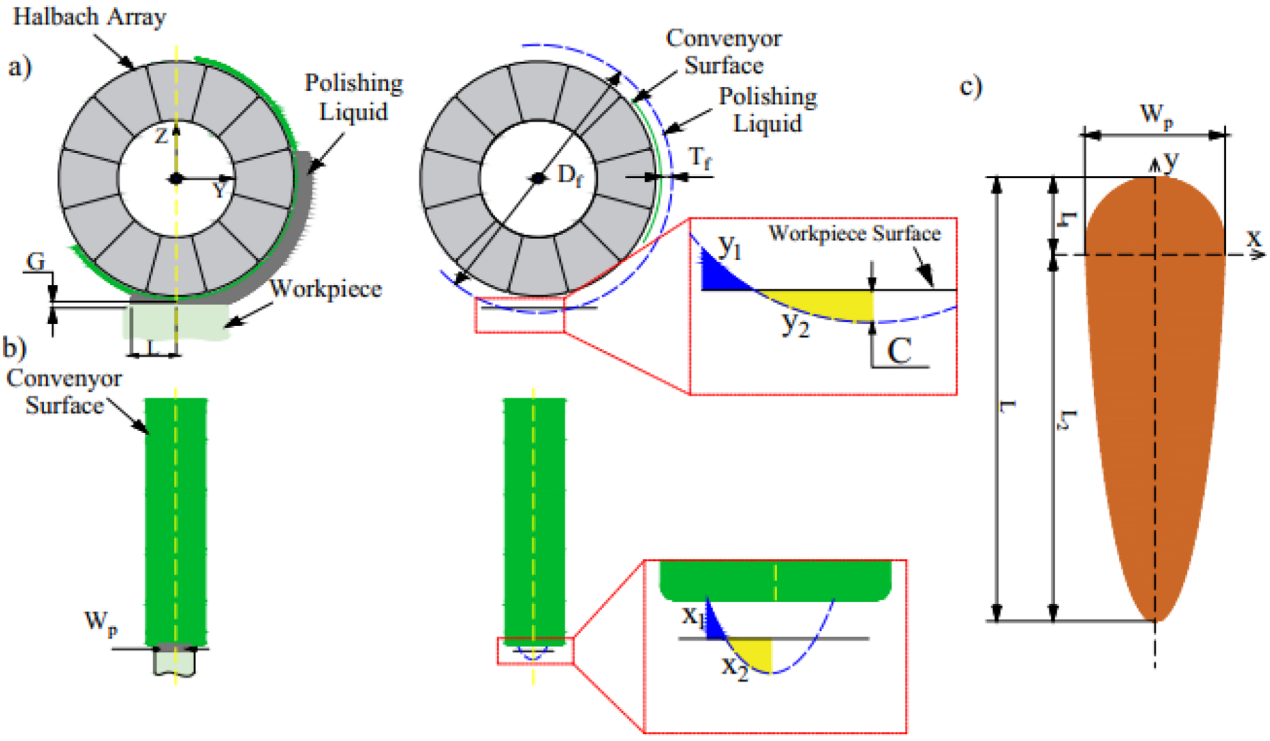

Fig. 10. Schematic illustration of (a) fluid compressed in the y direction, (b) fluid compressed in the x direction, (c) polished area.

bond between particles while grinding. carry out the process. From here we can confirm the effectiveness of Fe_3O_4@SiO_2 in the MRF polishing process. Using Fe_3O_4@SiO_2 as an abrasive can completely create an extremely bright and smooth nanometer-level material surface without causing any damage to the surface. This also means that in accordance with the mentioned operating principle, with the support of the abrasive replacement system and Halbach array, Fe_3O_4@SiO_2 can completely come into contact with the workpiece surface and be removed. Remove excess material. The reactions occurring on the Sapphire surface can be delineated as follows [41,42]:

$$H_2O + Al_2O_3 \rightarrow 2AlOOH, \tag{7}$$

$$H_2O + 2SiO_2 + Al_2O_3 \rightarrow Al_2Si_2O_7{\cdot}2H_2O, \tag{8}$$

$$SiO_2 + Al_2O_3 \rightarrow Al_2SiO_5. \tag{9}$$

4.2 Characteristics of material removal behavior of Fe_3O_4@SiO_2

In MRF processes, the shear stress in the machining area is mainly analyzed through determining the shear stress in the machining area, which is also the main influencing factor on the material removal activity of the process [29]. The analysis of cutting pressure should be considered during the analysis of material removal operations [30]. In this study, in order to understand the factors related to shear stress in the machining area generated by Fe_3O_4@SiO_2 abrasive particles are considered and outlined through theory and simulation.

4.2.1 Polishing area

Prior to analyzing the pressure distribution in the polishing region, it is imperative to delineate the boundaries of this area. The polishing zone is defined by the points of contact between the polishing tool and the workpiece surface, resulting in a shape akin to that of the polishing tool. Following the magnetic field analysis outlined in Section 3, it becomes evident that the polishing area assumes an elliptical shape. However, during the polishing process, the polishing solution undergoes compression, resulting in a deviation from a perfect ellipse. Figures 10a and 10b depict schematics of the compressed fluid within the polishing area.

Before establishing the stress field distribution within the polishing zone, it is essential to identify the boundaries of the polishing spot under different process parameters. When the MR fluid enters the magnetic field, it forms a magnetic ribbon consisting of iron powder particles. This magnetic ribbon is incompressible and will expand into the shapes depicted in Figures 10a and 10b. We examined the changes in the polishing bou`ndary resulting from variations in the immersion depth of the MRF ribbon. The y_2 value in Figure 10a can be determined using equation (6):

$$y_2^2 = \left(\frac{D_f}{2}\right)^2 - \left(\frac{D_f}{2} - C\right)^2. \tag{10}$$

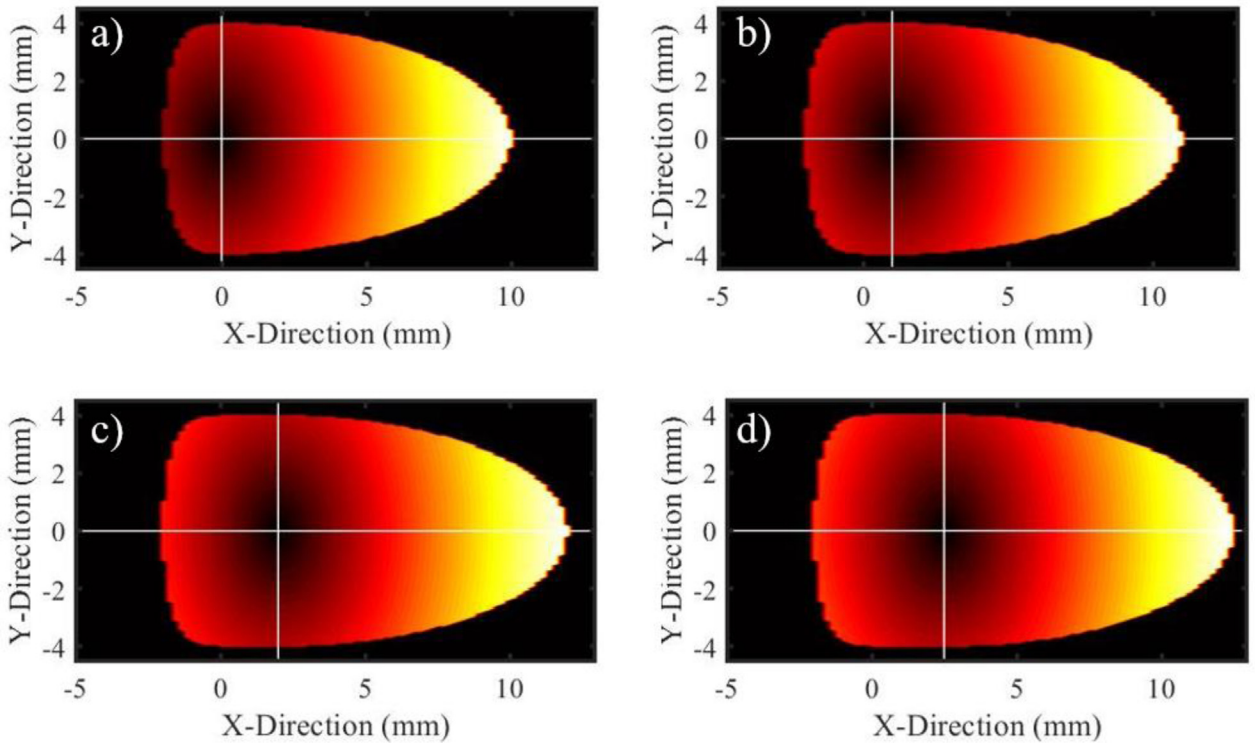

Fig. 11. Polishing area at working distances (a) $G = 0.7$ (mm); (b), $G = 1.2$ (mm); (c) $G = 1.6$ (mm); (d) $G = 2.0$ (mm).

As shown in the diagram from Figure 11, the polishing area is formed from different zones. For areas y_2 and y_1, their magnitude is determined through the following formula:

$$q = y_2 - y = \frac{D_f}{2} - C - \sqrt{\left(\frac{D_f}{2}\right)^2 - (y_2)^2}. \quad (11)$$

$$\left(\int_{y_1}^{y_2} q dy\right) = -\left(\int_{y_2}^{0} q dy\right), \quad (12)$$

where D_f *is* the diameter (mm) of the polishing tool and C the contact area depth (mm).

From here the length of the polished area can be calculated through the following formula:

$$L = |y_2|. \quad (13)$$

The width of the polished area (W_p) can be calculated similarly to the process of determining the length of the polished area (L) in case the pressure outside the polished area is 0. From here it is possible to build a profile of the polished area through the geometric method, the results are shown in Figure 10c. This region is divided into two parts, the rear part and the front part are defined through formulas (14) and (15), respectively:

$$x^2 \frac{1}{\left(\frac{W_p}{2}\right)^2} + \frac{(y + L_1)^2}{(L_1)^2} \leq 1 \left\{ x \in \left[\frac{-W_p}{2}; \frac{W_p}{2}\right], y \in [-L_1; 0) \right\}, \quad (14)$$

Table 2. Polishing area experiments with different working distances.

G (mm)	W_p (mm)	L (mm)
0.7	7.38	12.13
1.2	7.65	12.67
1.6	7.73	13.25
2.0	7.84	13.78

$$x^2 \frac{1}{\left(\frac{W_p}{2}\right)^2} + \frac{(y + L_1)^2}{(L_2)^2} \leq 1 \left\{ x \in \left[\frac{-W_p}{2}; \frac{W_p}{2}\right], y \in [-L_2; -L_1) \right\}, \quad (15)$$

where L_1 and L_2 are the length from the bottom to the center and from the center to the beginning of the polished area, respectively, W_p is the width of the polished area.

4.2.2 Shear stress in the polished zone

For liquid mixtures in polishing processes, its viscosity is not a constant but depends on other parameters: particle density, flow rate, etc. [10]. This also means that the polishing liquid mixture is non-Newtonian. In this context, the shear stress in the polishing area generated by the tool on the workpiece surface from Fe_3O_4@SiO_2 particles can be determined through the Reynolds equation [43]. In this case, the Reynolds equation is described as follows (16):

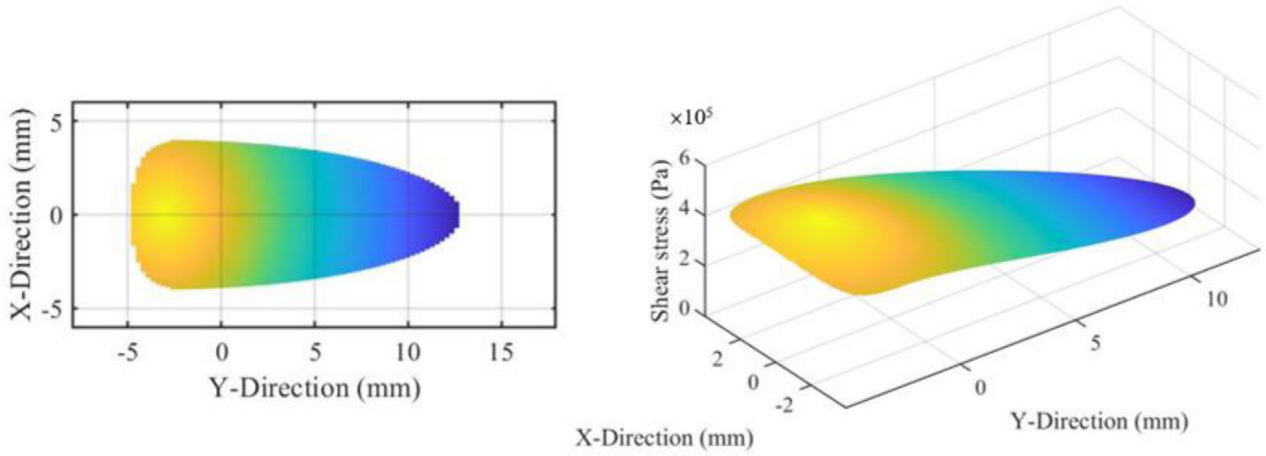

Fig. 12. Shear stress in the polished area.

Table 3. Experimental setup.

Parameters	Value	Material	Note
Workpiece		Sapphire	Size: 20 x 10 mm
Workpiece velocity	60 rpm		
Linear speed of conveyor belt	150 mm/s		
Working distance	$G = 0.7$ (mm); $G = 1.2$ (mm); $G = 1.6$ (mm); $G = 2.0$ (mm)		
Magnetic field supply method			Halbach array
MRF fluid mixture		Fe_3O_4@SiO_2: 40%;	Deionized water: 60%
Flow rate	15 ml/min		
Processing time	100 min		

$$\frac{\partial}{\partial y}\left(\frac{G^3}{\eta}\frac{\partial p}{\partial y}\right)+\frac{\partial}{\partial x}\left(\frac{G^3}{\eta}\frac{\partial p}{\partial y}\right)=6V\frac{\partial G}{\partial y}, \tag{16}$$

where G is the working distance (mm), V is the relative speed of the conveyor belt (rpm), p is the shear stress in the area.

In summary, the final finished surface of the workpiece is formed under repeated removal operations. From the polishing area determined in the previous section together with equation (13), the shear stress in the polishing area of the proposed process can be calculated. In MRF process, working distance (G) is one of the parameters that greatly affects the ball fighting process, adjusting this parameter can improve the surface quality as well as improve the ability remove material [44,45]. This distance is calculated from the outside point of the polishing tool to the workpiece surface. For areas with higher cutting pressure, it means that the removal of excess material is more active, which is also related to the polishing points as analyzed. When moving away from the center of the polishing area, the abrasive grain is no longer compressed, the cutting pressure gradually becomes weaker. Besides, as G gradually diminishes, the amount of compressed abrasive grain in the center of the polishing area increases, causing the cutting pressure to become larger, and more controlling. This is also completely reasonable with the previous analysis of batting scores. This parameter can be determined through formula (13). In case the liquid injection flow rate is fixed, meaning the liquid thickness (T_f) does not change, changing the working distance also means changing the contact area depth (C).

$$G = T_f - C. \tag{17}$$

To understand the effect of working distance on the change of the polishing area. An experiment analyzing polished areas with different working distances was carried out. The experiment is described as in Table 2. By determining the Reynolds equation and the polishing area,

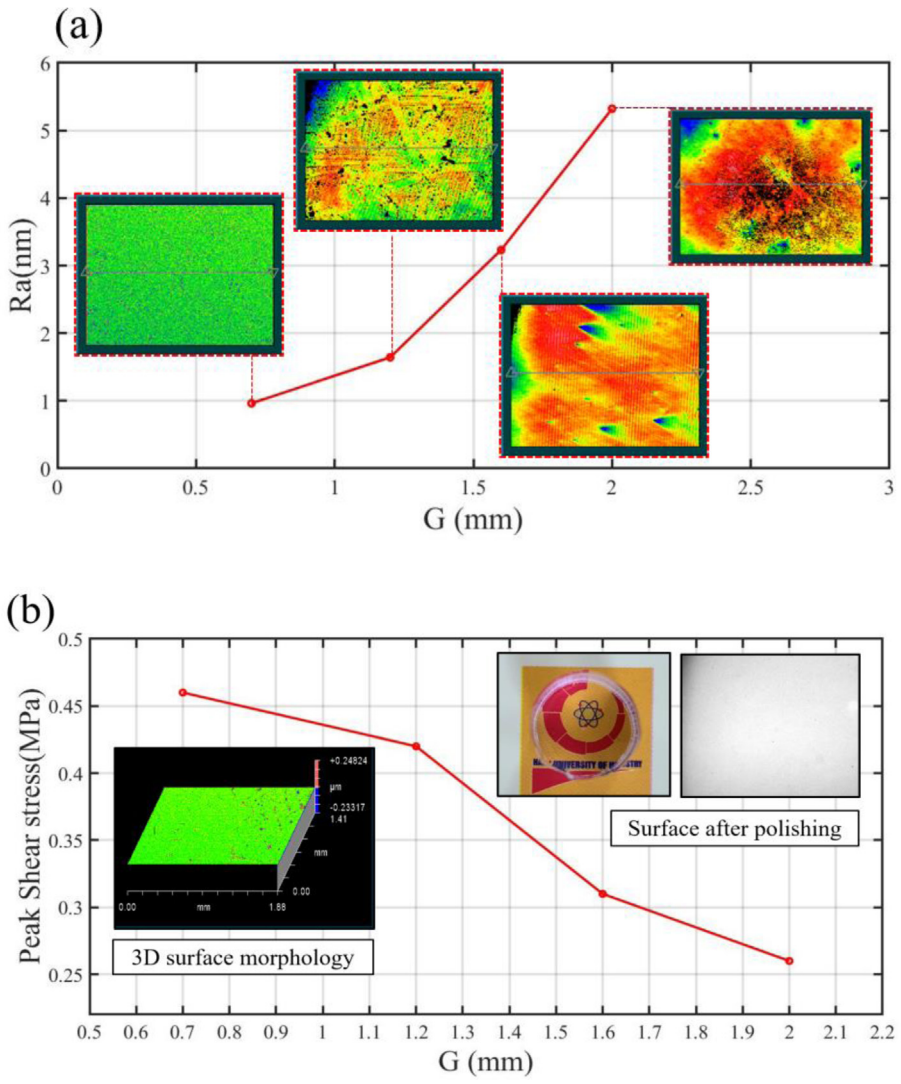

Fig. 13. Working distance affects (a) surface quality, (b) maximum shear stress in the area.

we can derive the pressure and shear force field distribution by solving the Reynolds equation (12). In the MRF experiments, the distribution of force fields is influenced by the process parameters and the properties of the MR fluid. This study considers the effects of three key parameters: immersion depth, MR fluid viscosity, and the rotational speed of the polishing wheel with the calculated removal function profiles as present in Figures 11a–11d. From the results that can be seen for different working distances, the polishing area also changes accordingly. In Figure 11, darker colours represent areas with denser polishing points. As G gradually decreases, the center of the hitting area also moves back and the hitting spots also become denser. This is explained by the fact that as G decreases, the polishing solution is compressed more at the center of the polishing area. So it can be concluded that as the working distance gradually decreases, material removal becomes more aggressive. The findings, depicted in Figure 12, suggest that shear stress is more pronounced in regions where the polishing solution mixture experiences compression, gradually diminishing as one moves away from this zone.

As discussed in the preceding section, alterations in the working distance (G) correspondingly modify the polishing area. In this regard, an experiment was conducted to investigate the impact of the working distance on the proposed MRF process. Table 3 outlines the experimental parameters. Figure 13a illustrates the influence of the working distance on the final surface quality, while Figure 13b depicts the variation of maximum shear stress within the polishing area with changes in the working distance. Analysis of the results from Figure 13a indicates that as G decreases, there is a notable improvement in surface quality. This improvement can be attributed to the larger shear stress in the area associated with smaller G values (as observed in Fig. 13b), signifying a more active removal of excess material. Consequently, surface roughness gradually increases with an increase in the working

distance, with the optimal surface quality achieved at $G = 0.7$ mm.

5 Conclusion

This paper introduces a novel MRF polishing process employing Fe_3O_4@SiO_2 nanomaterials as abrasives, complemented by the application of a Halbach array and an abrasive replacement system. Through theoretical analyses and finite element simulations, it is demonstrated that under the influence of the Halbach array, Fe_3O_4@SiO_2 abrasive particles aggregate into domelike clusters, facilitating efficient and robust contact with the material surface for material removal mechanisms. The abrasive replacement system ensures continuous renewal of Fe_3O_4@SiO_2 particles within the polishing area, eliminating issues associated with weak particle bonding observed in previous MRF processes.

Experimental validation using Sapphire material confirms the feasibility of utilizing Fe_3O_4@SiO_2 abrasives for achieving exceptionally bright and defect-free surfaces across various materials. The processed Sapphire surface exhibits nanometer-level roughness (Ra = 1.145 nm). Additionally, an analysis of the polishing area generated by the proposed MRF process reveals its dynamic nature, with changes in the working distance influencing material removal dynamics and final surface quality. Specifically, decreasing the working distance enhances material removal activity, leading to improved surface quality. The associated shear stress within the polishing area is also investigated, showing an increase in maximum stress as the working distance decreases. The optimal working distance for maximizing polishing efficiency is determined to be $G = 0.7$ mm.

Polishing using regenerated Fe_3O_4@SiO_2 abrasives in conjunction with a Halbach array holds significant promise for enhancing surface quality, even for challenging-to-machine materials like sapphire. In future research, we plan to apply the proposed model to the surface finishing of other difficult-to-machine materials, including titanium alloys, SUS 304 stainless steel, K9 optical glass, YAG crystals, and additional materials that present machining challenges. By doing so, we aim to assess the model's high applicability and effectiveness in industrial settings for processing these challenging materials.

Funding

This research received no external funding.

Conflicts of interest

The authors declare that they have no known competing financial interests or personal relationships that could have appeared to influence the work reported in this paper.

Data availability statement

The data that support the findings of this study are available on request from the corresponding author.

Author contribution statement

Nguyen Ngoc Quan: Conceptualization, Methodology, Software, Validation, Formal analysis, Investigation, Resources, Data Curation, Writing - Original Draft, Writing - Review & Editing, Visualization, Supervision, Project administration, Funding acquisition. Nguyen Minh Quang: Investigation, Resources, Data Curation, Writing - Review & Editing, Visualization. Le Thi Phuong Thanh: Investigation, Resources, Data Curation, Writing - Review & Editing, Visualization. Nguyen Tien Tung: Investigation, Resources, Data Curation, Writing - Review & Editing, Visualization. Tran Ngoc Tan: Investigation, Resources, Data Curation, Writing - Review & Editing, Visualization. Nguyen Duy Trinh: Conceptualization, Methodology, Software, Validation, Formal analysis, Investigation, Resources, Data Curation, Writing - Original Draft, Writing - Review & Editing, Visualization, Supervision, Project administration, Funding acquisition.

Informed consent

The authors declare that there are no potential conflicts of interest regarding the publication of this article.

References

1. U. Sellgren, S. Andersson, The concept of functional surfaces as carriers of interactive properties (2005), pp. 15–18
2. L. Nagdeve, V.K. Jain, J. Ramkumar, Nanofinishing of freeform/sculptured surfaces: state-of-the-art, Manufacturing Rev. **5** (2018), doi: 10.1051/mfreview/2018005
3. M. Ramezani, Z. Mohd Ripin, T. Pasang, C.-P. Jiang, Surface engineering of metals: techniques, characterizations and applications, Metals **13** (2023)
4. M. Vishnoi, P. Kumar, Q. Murtaza, Surface texturing techniques to enhance tribological performance: a review, Surf. Interfaces **27** (2021) 101–463
5. Z.-W. Zhong, Advanced polishing, grinding and finishing processes for various manufacturing applications: a review, Mater. Manufactur. Process. **35** (2020) 1279–1303
6. N.T. Duy, D.H. Tien, P.T.T. Thoa, A new environment-friendly magnetorheological finishing and fuzzy grey relation analysis in Ti-6Al-4V alloy polishing, Manufactur. Rev. **9** (2022), doi: 10.1051/mfreview/2022013
7. L.A. Duc, P.M. Hieu, N. Minh Quang, Development of OCMNO algorithm applied to optimize surface quality when ultra-precise machining of SKD 61 coated Ni-P materials, Manufacturing Rev. **10** (2023), doi: 10.1051/mfreview/2023006
8. T.S. Bedi, A.K. Singh, Magnetorheological methods for nanofinishing – a review, Particul. Sci. Technol. **34** (2016) 412–422
9. Y. Yang et al., A magnetic abrasive finishing process with an auxiliary magnetic machining tool for the internal surface finishing of a thick-walled tube, Machines **10** (2022)
10. A. Sidpara, M. Das, V.K. Jain, Rheological characterization of magnetorheological finishing fluid, Mater. Manufactur. Process. **24** (2009) 1467–1478

11. K. Saraswathamma, S. Jha, V.R. Paruchuri, Rheological behaviour of magnetorheological polishing fluid for Si polishing, Mater. Today: Proc. **4** (2017) 1478–1491
12. A. Muhammad, X. Yao, C. Deng, Review of magneto-rheological (MR) fluids and its applications in vibration control, J. Marine Sci. Appl **5** (2006) 17–29
13. R. Catrin, J. Neauport, D. Taroux, P. Cormont, C. Maunier, S. Lambert, Magnetorheological finishing for removing surface and subsurface defects of fused silica optics, Opt. Eng. **53** (2014) 092010
14. A. Makridis, N. Maniotis, D. Papadopoulos, P. Kyriazopoulos, M. Angelakeris, A novel two-stage 3D-printed Halbach array-based device for magneto-mechanical applications, Magnetochemistry **10** (2024)
15. M.G. Lee, S.Q. Lee, D.-G. Gweon, Analysis of Halbach magnet array and its application to linear motor, Mechatronics **14** (2004) 115–128
16. A. Sarwar, A. Nemirovski, B. Shapiro, Optimal Halbach permanent magnet designs for maximally pulling and pushing nanoparticles, J. Magn. Magn. Mater. **324** (2012) 742–754
17. M. Hoyos, L. Moore, P.S. Williams, M. Zborowski, The use of a linear Halbach array combined with a step-SPLITT channel for continuous sorting of magnetic species, J. Magn. Magn. Mater. **323** (2011) 1384–1388
18. Z.Q. Zhu, D. Howe, Halbach permanent magnet machines and applications: a review, IEE Proc. Electric Power Appl. **148** (2001) 299–308
19. M. Tanase et al., Magnetic alignment of fluorescent nanowires, Nano Lett. **1** (2001) 155–158
20. D.H. Tien, N.D. Trinh, Novel hybrid chemical magneto-rheological fluid for polishing Ti-6Al–4V alloy, Mater. Manufactur. Process. 1–18
21. M. Xie, Z. An, J. Zhuang, Design an d experimental research of dynamic magnetic field device based on Halbach array in magnetorheological polishing, Int. J. Adv. Manufactur. Technol. **120** (2022) 5807–5822
22. H. Li, T. Li, End-effect magnetic field analysis of the Halbach array permanent magnet spherical motor, IEEE Trans. Magn. **54** (2018) 1–9
23. S. Feng, S. Yong, D. Yifan, P. Xiaoqiang, L. Shengyi, Magnetorheological elastic super-smooth finishing for high-efficiency manufacturing of ultraviolet laser resistant optics, Opt. Eng. **52** (2013) 075104
24. C. Qian, Y. Tian, S. Ahmad, Z. Ma, L. Li, Z. Fan, Theoretical and experimental investigation on magnetorheological shear thickening polishing force using multi-polecoupling magnetic field, J. Mater. Process. Technol. **328** (2024) 118–414
25. D. Cubero, L. Marmugi, F. Renzoni, Exploring the limits of magnetic field focusing: simple planar geometries, Res. Phys. **19** (2020) 103562
26. S.N. Shafrir et al., Zirconia-coated carbonyl-iron-particle-based magnetorheological fluid for polishing optical glasses and ceramics, Appl. Opt. **48** (2009) 6797–6810
27. J. Pan, Z. Chen, Q. Yan, Study on the rheological properties and polishing properties of SiO2@CI composite particle for sapphire wafer, Smart Mater. Struct. **29** (2020) 114003
28. Q. Zhai, W. Zhai, B. Gao, Y. Shi, X. Cheng, Synthesis and characterization of nanocomposite Fe_3O_4/SiO_2 core-shell abrasives for high-efficiency ultrasound-assisted magneto-rheological polishing of sapphire, Ceramics Int. **47** (2021) 31681–31690
29. H. Guo, Y. Wu, D. Lu, M. Fujimoto, M. Nomura, Effects of pressure and shear stress on material removal rate in ultra-fine polishing of optical glass with magnetic compound fluid slurry, J. Mater. Process. Technol. **214** (2014) 2759–2769
30. J. Liu, X. Li, Y. Zhang, D. Tian, M. Ye, C. Wang, Predicting the material removal rate (MRR) in surface magnetorheological finishing (MRF) based on the synergistic effect of pressure and shear stress, Appl. Surf. Sci. **504** (2020) 144492
31. E.D. Jessica, J.R. Henry, A.K. Irina, M.S. John, D.J. Stephen, Polishing PMMA and other optical polymers with magneto-rheological finishing, Proc. SPIE **5180** (2003) 123–134
32. C. Miao, S.N. Shafrir, J.C. Lambropoulos, J. Mici, S.D. Jacobs, Shear stress in magnetorheological finishing for glasses, Appl. Opt. **48** (2009) 2585–2594
33. L. Xiaojuan, J. Guoyuan, Z. Liping, Y. Yu-xiang, L. Xiangnong, Synthesis and properties of Fe_3O_4 nanoparticles by sol-vothermal method using iron(III) acetylacetonate, Glass Phys. Chem. **37** (2011)
34. I. Nyiro-Kosa, D. Nyinagy, M. Pósfai, Size and shape control of precipitated magnetite nanoparticles, Eur. J. Mineral. **21** (2009) 293–302
35. Y.Y. Zheng et al., Fabrication of shape controlled Fe_3O_4 nanostructure, Mater. Character. **61** (2010) 489–492
36. K. Mandel, C. Kolb, M. Straßer, S. Dembski, G. Sextl, Size controlled iron oxide nano octahedra obtained via sono-chemistry and natural ageing, Coll. Surf. A **457** (2014)
37. N. Duy Trinh, N.T. Nguyen, N. Minh Quang, T. Pham, L. Anh Duc, Particulate science and technology application of magnetic liquid slurries and fuzzy grey analysis in polishing nickel-phosphorus coated SKD11 steel Application of magnetic liquid slurries and fuzzy grey analysis in polishing nickel-phosphorus coated SKD11 steel, Particul. Sci. Technol. **39** (2021)
38. J.S. Choi, J. Yoo, Design of a Halbach magnet array based on optimization techniques, IEEE Trans. Magnetics **44** (2008) 2361–2366
39. J. O'Connell, W. Robertson, B. Cazzolato, Optimization of the magnetic field produced by frustum permanent magnets for single magnet and planar Halbach array configurations, IEEE Trans. Magn. (2021) 1–1
40. E.R. Dobrovinskaya, L.A. Lytvynov, V. Pishchik, Application of Sapphire, in Sapphire: Material, Manufacturing, Applications, edited by V. Pishchik, L.A. Lytvynov, E.R. Dobrovinskaya (Springer US, Boston, MA, 2009), pp. 1–54
41. Q. Zhai, W. Zhai, B. Gao, S. Yiqing, X. Cheng, Synthesis and characterization of nanocomposite Fe_3O_4/SiO_2 core-shell abrasives for high-efficiency ultrasound-assisted magneto-rheological polishing of sapphire, Ceram. Int. **47** (2021)
42. E. Vovk, A.T. Budnikov, M. Dobrotvorskaya, S.I. Krivonogov, D.A.Ya, Mechanism of the Interaction between Al_2O_3 and SiO_2 during the chemical-mechanical polishing of sapphire with silicon dioxide, J. Surface Invest. X-ray Synchrot. Neutron Tech. **6** (2012) 115–121
43. Y. Peiran, W. Shizhu, A generalized reynolds equation for non-Newtonian thermal elastohydrodynamic lubrication, J. Tribol. **112** (1990) 631–636

44. C. Kumari, S.K. Chak, Study on influential parameters of hybrid AFM processes: a review, Manufactur. Rev. **6** (2019), doi: 10.1051/mfreview/2019022

45. C. Kumari, S.K. Chak, A review on magnetically assisted abrasive finishing and their critical process parameters, Manufactur. Rev. **5** (2018), doi: 10.1051/mfreview/2018010

Cite this article as: Nguyen Ngoc Quan, Nguyen Minh Quang, Le Thi Phuong Thanh, Nguyen Tien Tung, Tran Ngoc Tan, Nguyen Duy Trinh, Synthesis nano core-shell material Fe_3O_4@SiO_2 for magnetorheological finishing with Halbach array and regenerative abrasive system, Manufacturing Rev. **11**, 18 (2024)